Biochemical and Biophysical Research Communications 449 (2014) 62–68

Contents lists available at ScienceDirect

Biochemical and Biophysical Research Communications

journal homepage: www.elsevier.com/locate/ybbrc

Novel distribution of calreticulin to cardiomyocyte mitochondria and its increase in a rat model of dilated cardiomyopathy

Ming Zhang [a,b], Jin Wei [a,*], Yali Li [b], Hu Shan [a], Rui Yan [a], Lin Lin [a], Qiuhong Zhang [b], Jiahong Xue [a]

[a] Department of Cardiology, Second Affiliated Hospital, School of Medicine, Xi'an Jiaotong University, Xi'an, Shaanxi, China
[b] Department of Respiratory Medicine, Second Affiliated Hospital, School of Medicine, Xi'an Jiaotong University, Xi'an, Shaanxi, China

ARTICLE INFO

Article history:
Received 27 April 2014
Available online 9 May 2014

Keywords:
Calreticulin
Mitochondria
Apoptosis
STAT3
Dilated cardiomyopathy

ABSTRACT

Background: Calreticulin (CRT), a Ca^{2+}-binding chaperone of the endoplasmic reticulum, can also be found in several other locations including the cytosol, nucleus, secretory granules, the outer side of the plasma membrane, and the extracellular matrix. Whether CRT is localized at mitochondria of cardiomyocytes and whether such localization is affected under DCM are still unclear.
Methods and results: The DCM model was generated in rats by the daily oral administration of furazolidone for thirty weeks. Echocardiographic and hemodynamic studies demonstrated enlarged left ventricular dimensions and reduced systolic and diastolic function in DCM rats. Immuno-electron microscopy and Western blot showed that CRT was present in cardiomyocyte mitochondria and the mitochondrial content of CRT was increased in DCM hearts ($P < 0.05$). Morphometric analysis showed notable myocardial apoptosis and mitochondrial swelling with fractured or dissolved cristae in the DCM hearts. Compared with the control group, the mitochondrial membrane potential level of the freshly isolated cardiac mitochondria and the enzyme activities of cytochrome c oxidase and succinate dehydrogenase in the model group were significantly decreased ($P < 0.05$), and the myocardial apoptosis index and the caspase activities of caspase-9 and caspase-3 were significantly increased ($P < 0.05$). Pearson linear correlation analysis showed that the mitochondrial content of CRT had negative correlations with the mitochondrial function, and a positive correlation with myocardial apoptosis index ($P < 0.001$). The protein expression level of cytochrome c and the phosphorylation activity of STAT3 in the mitochondrial fraction were significantly decreased in the model group compared with the control group ($P < 0.05$).
Conclusions: These data demonstrate that CRT is localized at cardiomyocyte mitochondria and its mitochondrial content is increased in DCM hearts.

1. Introduction

Dilated cardiomyopathy (DCM) is characterized mainly by left ventricular systolic dysfunction (abnormality of contraction), with an associated increase in mass and volume, and has many causes [1]. However, the mechanisms and pathogenesis of DCM are still poorly understood. Cardiac mitochondria are the energy power for heart systolic and diastolic function, and obvious structural and functional damage of the cardiac mitochondria are present in the patients with DCM [2]. Therefore cardiac mitochondrial molecular abnormalities constitute an attractive basis of the development of DCM.

Calreticulin (CRT) is a Ca^{2+}-binding chaperone of the endoplasmic reticulum involved in Ca^{2+} storage and modulation of intracellular Ca^{2+} homeostasis [3]. CRT is highly expressed in the embryonic heart, but immediately down-regulated after birth [4]. The overexpression of CRT in the postnatal mouse heart results in DCM, but the mechanism is not fully understood [5]. Moreover, the alterations of CRT expression in DCM hearts remain ambiguous [6,7].

Although it is generally assumed that CRT is exclusively localized in the sarcoplasmic reticulum [3], there is some evidence that this may not be the case. Recent studies have shown that CRT can also be found in several other locations including the cytosol [8,9], nucleus [10,11], secretory granules [12,13], the outer side of the plasma membrane [14], and the extracellular matrix [15].

Since mitochondria play an important role in the development of DCM, the aims of the present study were to investigate whether CRT is localized at rat cardiomyocyte mitochondria, and whether the mitochondrial content of CRT is altered in the DCM rat hearts.

* Corresponding author. Address: Department of Cardiology, The Second Affiliated Hospital, School of Medicine, Xi'an Jiaotong University, 157 West Fifth Road, Xi'an, Shaanxi 710004, China. Fax: +86 029 87679775.
E-mail address: weijindr@163.com (J. Wei).

http://dx.doi.org/10.1016/j.bbrc.2014.04.156
0006-291X/

2. Materials and methods

2.1. Materials

Sprague–Dawley rats (male, 2 weeks old) were purchased from Animal Center of Xi'an Jiaotong University (Xi'an, China). All the chemicals and reagents were purchased from Sigma unless otherwise mentioned.

2.2. Animal model

A model of DCM was generated in Sprague–Dawley rats through administrating furazolidone solution (700 ppm) as described previously [16]. The rats in the control group drank 0.15% carboxy methylcellulose-Na solution, and the untreated group drank tap water only. All animal study protocols were approved by the Institutional Animal Research and Ethics Committee of Xi'an Jiaotong University (SCXK2007-001).

2.3. Hemodynamic and echocardiographic measurements

After anesthetizing rats by intraperitoneal injection of chloral hydrate (300 mg/kg), two-dimensional, targeted M-mode tracings were obtained at the level of the papillary muscles with an echocardiographic system (Philips iE33) equipped with a 12–4 MHz transducer (Philips). A series of cardiac parameters including the Tei index [17], were measured and calculated. Then, a PE-50 catheter connecting a pressure-electricity transducer was inserted into the right carotid artery and advanced into the left ventricle (LV) to record left ventricular systolic and diastolic pressures, as well as the maximum and minimum rates of LV pressure development (dP/dt), using the Power Lab 4.12 system (AD instrument, Sydney, Australia). All studies were performed by an investigator blinded to the treatments, and each measurement was obtained with an average of three consecutive heart beats.

2.4. Ultrastructure analysis

Fresh tissue from the apex of the hearts was cut into pieces $1mm^3$, fixed with 2.5% glutaraldehyde, then fixed with 1% perosmic acid and dehydrated in an ethanol series. Ultrathin sections were placed on 400 mesh grids and double-stained with uranyl acetate and lead citrate, then observed with a transmission electron microscope (HITACHI-H7650, Tokyo, Japan).

2.5. Immuno-electron microscopy

Rats were anesthetized, and then fresh tissue from the apex of the hearts was fixed in 0.5% glutaraldehyde and 4% paraformaldehyde in 0.1 M sodium phosphate buffer pH7.4 at 4 °C for 2 h. Samples were then dehydrated in ethanol and embedded in Lowicryl K4M at low temperature. Ultrathin sections were cut and placed on formvar-coated 100-mesh nickel grids. The sections were first blocked with 1% bovine serum albumin (BSA) at room temperature for 30 min, and then incubated at 4 °C overnight with the primary antibody, rabbit anti-CRT (Abcam) at a dilution of 1:500. After washing, sections were detected with a secondary antibody coated with 10-nm colloidal gold, and subsequently the grids were double-stained with uranyl acetate and lead citrate. As a control, samples were prepared without the primary antibody. The sections were examined under a transmission electron microscope at 80 kV.

2.6. TUNEL assay

DNA fragmentation of myocardial cells was detected in situ by terminal deoxyribonucleotide transferase-mediated dUTP nick end labeling (TUNEL) with the In Situ Cell Death Detection Kit, Fluorescein (Roche Molecular Biochemicals). The LV myocardia were fixed in 10% neutral buffered formalin, and paraffin sections were then cut. The sections were pretreated with proteinase K working solution at 37 °C for 10 min, and subsequently permeabilized in a solution containing 0.1% Triton X-100 in 0.1% sodium citrate at 37 °C for 8 min, followed by incubation in the freshly prepared TUNEL reaction mixture for 90 min at 37 °C in the dark. The sections were then washed with PBS and counterstained with 4′,6′-diamidino-2-phenylindole (DAPI). Finally the sections were washed again with PBS and treated with anti-fading solution. Photographs were taken with a fluorescence microscope (Leica Company, Germany). Six high power fields were randomly sampled and positive cells were calculated for every section and five sections from each group.

2.7. Mitochondria isolation

Cardiac mitochondria were isolated from rat hearts as previously described using some modifications [18,19]. Nuclei and unbroken cells were pulled down by centrifugation at 1000*g* for 10 min at 4 °C. Then, the mitochondrial fraction was obtained by centrifugation of supernatant at 10,000*g* for 10 min at 4 °C, and purified by 30% percoll gradient ultracentrifugation at 45,000*g* for 50 min at 4 °C. The purified cardiac mitochondria were suspended in mitochondrial storage fluid (300 mmol/L sucrose, 2 mmol/L Hepes, 0.1 mmol/L EGTA, pH7.4), and stored at −80 °C. The purified cardiac mitochondria were confirmed by the transmission electron microscope examination. The purification procedure was assessed as the enrichment in mitochondrial proteins as well as the elimination of other cellular constituents by means of Western-blot analysis.

2.8. JC-1 assay for mitochondrial membrane potential

Mitochondrial membrane potential (MMP) was assessed using the lipophilic cationic probe 5,5′,6,6′-tetrachloro-1,1′,3,3′-tetraethylbenzimidazolylcarbocyanine iodide (JC-1). For quantitative fluorescence measurements, isolated fresh mitochondria were rinsed once after JC-1 staining and scanned with a fluorescence microplate reader (Tecan Infinite M200, Switzerland) at 490 nm excitation and 590 nm emission to measure red JC-1 fluorescence. Each well was scanned by measuring the intensity of each of 25 squares (of 1 mm^2 area) arranged in a 5×5 rectangular array.

2.9. Measurements of mitochondrial enzyme activities

Cytochrome c oxidase (COX) and succinate dehydrogenase (SDH) activities were measured using a COX assay kit (Genemed Scientifics Inc., Shanghai, China) and SDH assay kit (Jiancheng Bioengineering Co., Nanjing, China) following the manufacture's instructions, as previously described [16].

2.10. Measurements of caspase-3 and caspase-9 activities

Caspase-3 and caspase-9 activities were measured using the kits (Beyotime) following the manufacturer's instructions. Briefly, the myocardial tissue homogenates were incubated in a 96-well microtitre plate with 20 ng Ac-DEVD-pNA (caspase-3 activity) or Ac-LEHD-pNA (caspase-9 activity) for 2 h at 37 °C. Caspase activity was measured by cleavage of the Ac-DEVD-pNA or Ac-LEHD-pNA substrate to pNA, the absorbance of which was measured at 405 nm. Relative caspase activity was calculated as a ratio of untreated group.

Table 1
Hemodynamic and echocardiographic analysis.

Parameter	Untreated	Control	Model
Echocardiographic data			
Number	6	9	16
HR (beats/min)	393 ± 26.9	413 ± 38.8	392 ± 42.4
LVDd (mm)	6.97 ± 0.16	7.05 ± 0.18	7.74 ± 0.42*
LVDs (mm)	4.06 ± 0.15	4.02 ± 0.13	5.04 ± 0.21*
IVST (mm)	1.56 ± 0.06	1.57 ± 0.16	1.52 ± 0.15
PWT (mm)	1.39 ± 0.09	1.39 ± 0.18	1.23 ± 0.13*
LVEDV(μl)	253 ± 13.1	259 ± 15.2	321 ± 39.0*
LVESV (μl)	72.5 ± 6.49	70.9 ± 5.59	120 ± 12.2*
FS (%)	41.8 ± 1.84	42.94 ± 1.52	34.86 ± 2.72*
EF (%)	71.4 ± 1.06	72.6 ± 1.71	62.3 ± 3.64*
Tei index	0.37 ± 0.05	0.36 ± 0.06	0.73 ± 0.09*
Hemodynamic data			
Number	6	6	10
dP/dt_{max} (mmHg/s)	8406 ± 855	8668 ± 723	5258 ± 500*
dP/dt_{min} (mmHg/s)	7463 ± 820	7559 ± 1093	4951 ± 744*
LVSP (mmHg)	139 ± 8.86	135 ± 8.49	111 ± 15.8*
LVEDP (mmHg)	−1.42 ± 0.33	−1.34 ± 0.45	2.46 ± 0.78*

Values are mean ± SD. HR, heart rate; LVDd, left ventricular end-diastolic dimension; LVDs, left ventricular end-systolic dimension; IVST: inter-ventricular septal thickness; PWT: posterior wall thickness; LVEDV: left ventricular end-diastolic volume; LVESV: left ventricular end-systolic volume; FS, fractional shortening; EF, ejection fraction; *dp*/*dt*, first derivative of pressure; LVSP, left ventricular systolic pressure; LVEDP, left ventricular end-diastolic pressure.
* $P < 0.05$ versus the control group.

2.11. Western-blot analysis

Samples were lysed with RIPA lysis buffer containing protease and phosphatase inhibitors (Roche, Germany). The lysates were homogenized and the homogenates were centrifuged at 16,000*g* for 20 min at 4 °C. The supernatants were collected and protein concentrations were determined. Equivalent amounts of protein were subjected to sodium dodecyl sulfate–polyacrylamide gel electrophoresis and transferred onto a polyvinylidene difluoride membrane (Millipore). The membranes were incubated with specific antibodies against CRT (1:1500; Abcam), STAT3 (1:2000; Cell Signaling), phosphorylated STAT3 (Tyr705; 1:1000; Cell Signaling), cytochrome c (1:500; Proteintech), Na^+/K^+-ATPase (1:1000; Epitomics), sarcoplasmic calcium-ATPase (SERCA2; 1:1000; Epitomics), Gαs (1:500; Santa Cruz), lamin A (1:500; Santa Cruz), voltage-dependent anion channels (VDAC; 1:800; Proteintech), and cytochrome c oxidase subunit IV (COXIV; 1:2500; Cell Signaling). Blots were visualized with a secondary antibody coupled to horseradish peroxidase (Pierce Biotechnology) and an enhanced chemiluminescence detection system (Pierce Biotechnology). In this experiment, COXIV was used as a loading control for the mitochondrial protein.

2.12. Statistical analysis

All data are presented as mean ± standard deviation (SD) and were analyzed using SPSS 16.0 software. Analysis of data was performed using one-way analysis of variance test and LSD test. The correlations between mitochondrial content of CRT and cardiac mitochondrial function or myocardial apoptosis index were analyzed using Linear regression and correlation analysis. $P < 0.05$ was considered statistically significant.

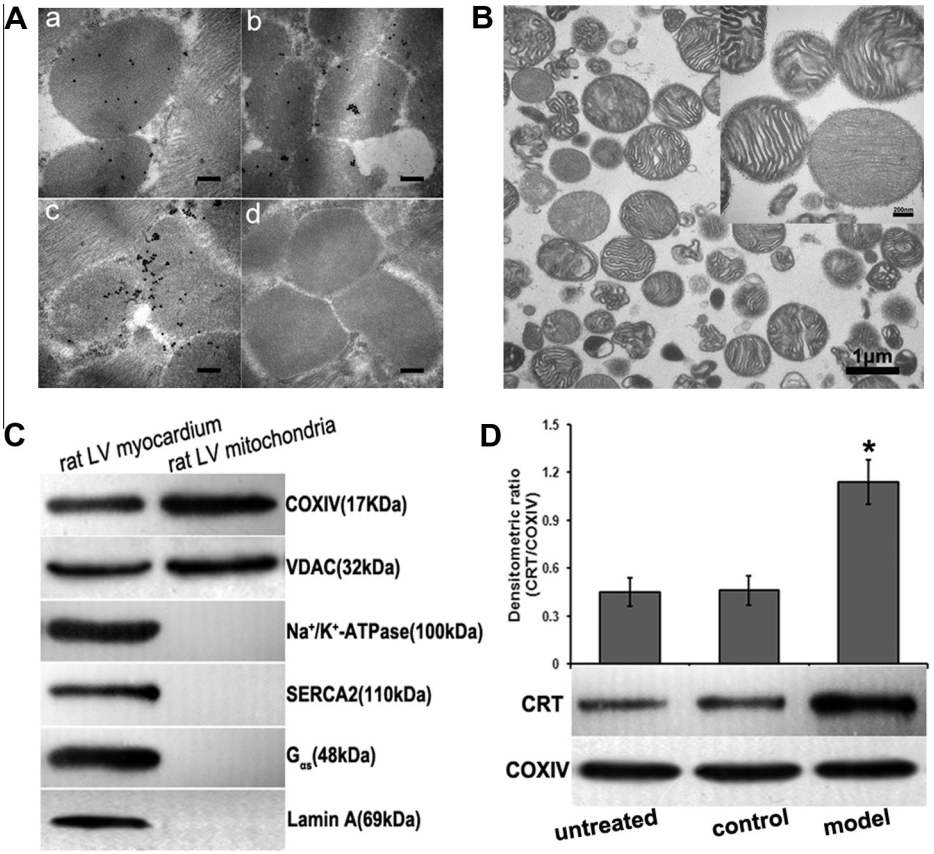

Fig. 1. CRT is present in rat left ventricular mitochondria. (A) Representative images of immune-electron labeling of CRT in cardiomyocyte mitochondria from untreated (a), control (b) and model (c) groups were shown. In (d), the primary antibody was omitted as a negative control. Scale bar = 200 nm. (B) Purified rat left ventricular mitochondria were observed under electron microscopy. (C) Western blot analysis further showed that no immunoreactive signals were detected for markers of the plasma membrane (Na^+/K^+-ATPase, $G_{\alpha s}$protein), the sarcoplasmic reticulum (SERCA2), the cytosol ($G_{\alpha s}$protein), and the nucleus (lamin A) in the mitochondrial extracts. (D) Mitochondrial content of CRT was detected by Western blot analysis. The protein expression is represented as the mean ± SD (n = 6, 6 and 10 respectively). *$P < 0.05$ versus the control group.

3. Results

3.1. Clinical course

After continuous furazolidone administration for thirty weeks, the rats showed inanimate behavior, decreased physical activity and food intake and an increased rate of breathing. Four out of twenty rats in the model group died, while no rats died in the control and untreated groups. Additionally, fourteen out of twenty rats in the model group were found with pericardial effusion, but no effusion occurred in the control and untreated groups. Peritoneal effusion has not been observed in any groups.

3.2. Echocardiographic and hemodynamic parameters

After furazolidone treatment for thirty weeks, echocardiographic studies on the rats in the model and control groups showed the evidence for cardiac remodeling in DCM hearts with increased LVDd and LVDs (7.74 ± 0.42 versus 6.97 ± 0.16 mm and 5.04 ± 0.21 versus 4.06 ± 0.15 mm, respectively, both $P < 0.05$), reduced %FS and %EF (34.86 ± 2.72 versus 41.8 ± 1.84 and 62.3 ± 3.64 versus 71.4 ± 1.06, respectively, both $P < 0.05$), and increased Tei index (0.73 ± 0.09 versus 0.37 ± 0.05, $P < 0.05$). At this time point, hemodynamic measurement obtained through intracardiac catheterization showed significantly reduced LVSP (111 ± 15.8 versus 139 ± 8.86 mmHg, $P < 0.05$) and impaired dP/dt in the model group compared with the control group. The rats in the untreated group had similar echocardiographic and hemodynamic parameters to those of the control group (Table 1).

3.3. Location of CRT at mitochondria

Ultrastructural immunolabeling was performed using the rabbit anti-rat CRT antibody to detect whether CRT is expressed in cardiac mitochondria. Immuno-electron analysis of myocardial samples from rat LV myocardium demonstrated the presence of colloidal gold-marked CRT antibodies at mitochondria in the untreated group, control group and model group (Fig. 1A), whereas no particles were detected in the negative control preparations in which the primary antibody had been omitted (Fig. 1A). More interestingly, there were more gold particles in the model group compared with the control group.

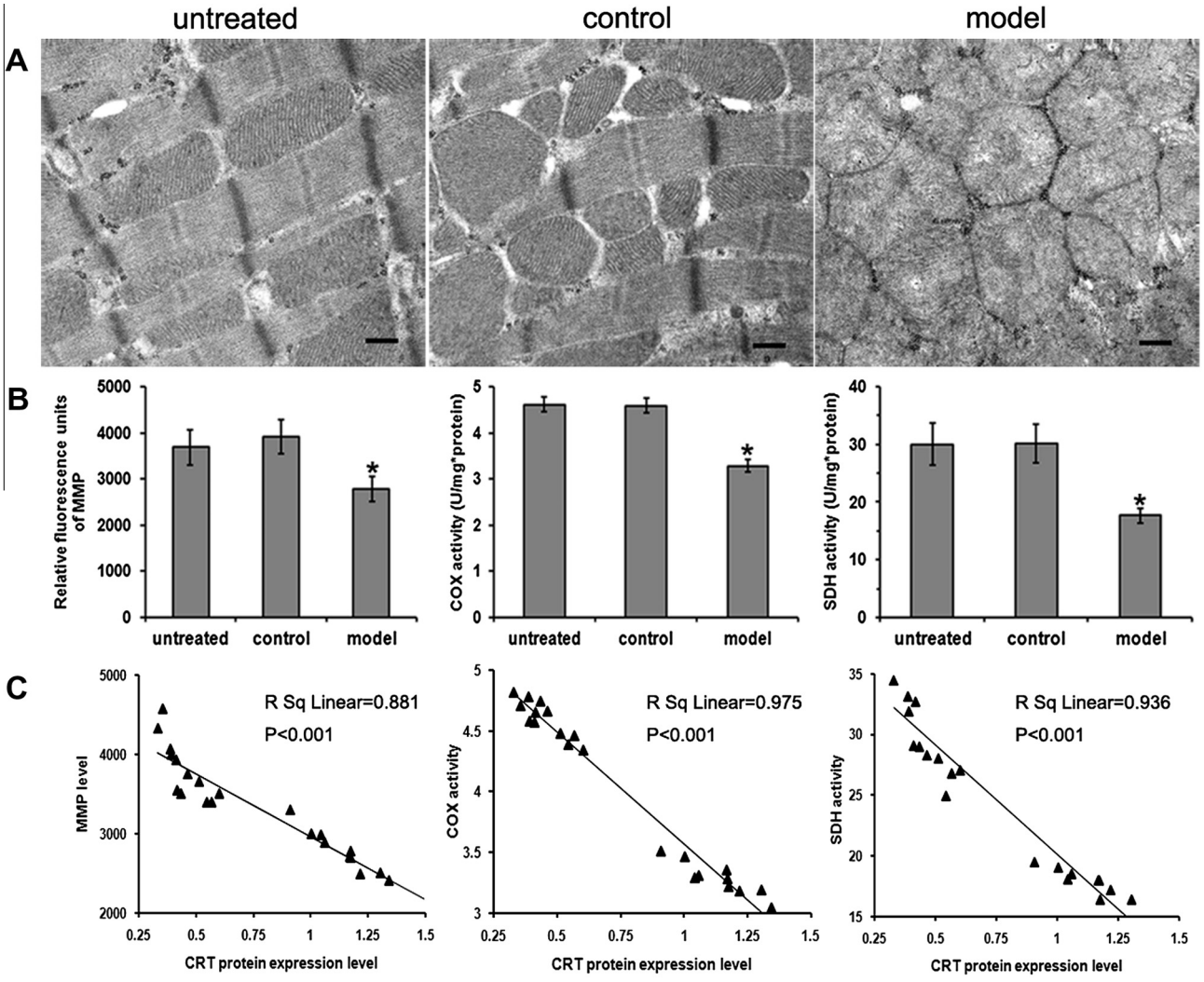

Fig. 2. Alterations of cardiac mitochondria and their correlations with mitochondrial content of CRT. (A) Normal mitochondrial structure was shown in the untreated and control groups, and swollen mitochondria with fractured or dissolved cristae in the model group. Scale bar = 250 nm. (B) Compared with the control group, the enzyme activities of COX (cytochrome c oxidase) and SDH (succinate dehydrogenase), and MMP (mitochondrial membrane potential) level in the isolated cardiac mitochondria in the model group significantly decreased. Data are mean ± SD ($n = 6$, 6 and 10 respectively). $^{*}P < 0.05$ versus the control group. (C) Mitochondrial content of CRT correlated negatively with the enzyme activities of COX and SDH, and the MMP level of the isolated cardiac mitochondria.

3.4. Increased mitochondrial content of CRT in DCM hearts

Cardiac mitochondria were extracted from the rat LV myocardium, and were purified through density gradient ultracentrifugation. Using electron microscopy, we observed that there were nearly no other cellular components except mitochondria in the extracts, and mitochondrial membrane was integrity (Fig. 1B). Western blot analysis further showed that no immunoreactive signals were detected for markers of the plasma membrane (Na^+/K^+-ATPase, $G_{\alpha s}$protein), the sarcoplasmic reticulum (SERCA2), the cytosol ($G_{\alpha s}$protein), and the nucleus (lamin A) in the mitochondrial extracts (Fig. 1C). In the mitochondrial extracts, which stained positive for markers of the mitochondria (COXIV and VDAC), CRT was present, and its protein expression level was significantly increased in the model group compared with the control group ($P < 0.05$, Fig. 1D). Moreover, the mitochondrial content of CRT did not differ between the untreated and control groups ($P > 0.05$).

3.5. Mitochondrial morphology and function

Using electron microscopy, we observed morphological changes of cardiomyocyte ultrastructure in the model group, including swollen mitochondria with fractured or dissolved cristae, vacuolization of the cytoplasm, and dilation of the sarcotubular system with irregular cell nuclei. However, the cardiomyocyte ultrastructure in the untreated and control groups showed regular myofibril arrangement, maintained sarcotubular systems, and preserved mitochondria (Fig. 2A). Compared with the control group, MMP level of the isolated fresh cardiac mitochondria in the model group

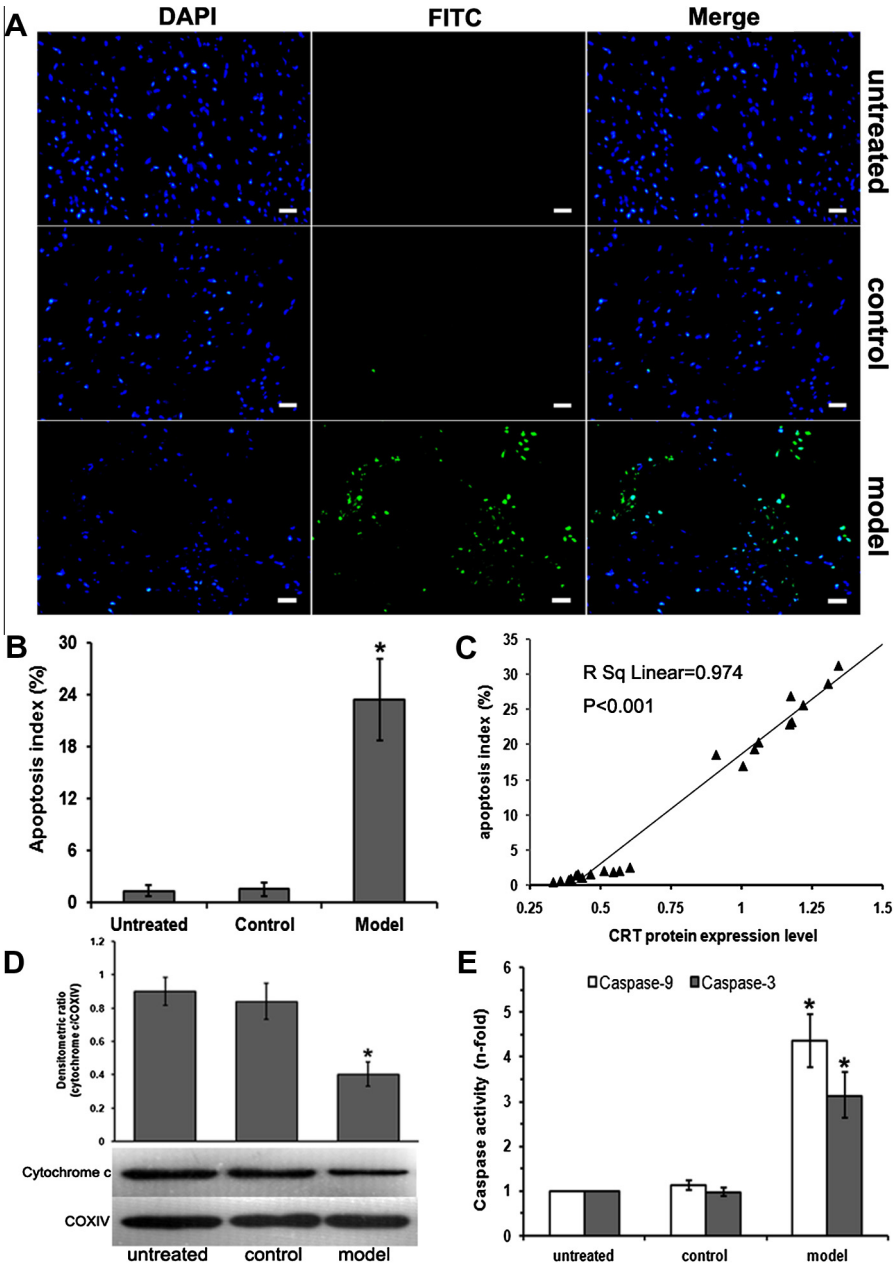

Fig. 3. Increased myocardial apoptosis in DCM rats. (A) Myocardial apoptosis was detected by TUNEL assay. Blue fluorescent spots represent all of nucleus, and green fluorescent spots represent the apoptotic cells. (B) The myocardial apoptosis index in the model group was significantly increased. (C) Mitochondrial content of CRT correlated positively with the myocardial apoptosis index. (D) Mitochondrial content of cytochrome c was detected by Western blot analysis. (E) Caspase 9/3 activities were detected by commercially available ELISA kits. Data are mean ± SD ($n = 6$, 6 and 10 respectively). $^*P < 0.05$ versus the control group. (For interpretation of the references to color in this figure legend, the reader is referred to the web version of this article.)

significantly decreased (77.1 ± 6.54% versus 95.66 ± 8.57%, $P < 0.05$, Fig. 2B). Moreover, the enzyme activities of COX and SDH in the model group were lower than those in the control group (72.7 ± 5.5% versus 102 ± 8.05% and 61.2 ± 5.7% versus 96.3 ± 8.01%, respectively, both $P < 0.05$, Fig. 2B). MMP, COX, and SDH did not differ between the untreated and control groups ($P > 0.05$). Pearson linear correlation analysis showed that the mitochondrial content of CRT had negative correlations with the MMP level and the enzyme activities of COX and SDH ($P < 0.001$, Fig. 2C).

3.6. Increased myocardial apoptosis in DCM rat

TUNEL assay demonstrated notable myocardial apoptosis occurred in the DCM rats (Fig. 3A), and quantitative analysis further revealed the myocardial apoptosis index in the model group was higher than that in the control group (23.4 ± 4.67 versus 1.52 ± 0.73, $P < 0.05$, Fig. 3B). Pearson linear correlation analysis showed that the mitochondrial content of CRT had positive correlation with the myocardial apoptosis index (linear correlation coefficient = 0.987, $P < 0.05$, Fig. 3C).

To further determine whether myocardial apoptosis was a mitochondrial-dependent pathway, we tested whether cytochrome c could be released from the mitochondria into the cytoplasm. As shown in Fig. 3D, the mitochondrial content of cytochrome c in the model group was significantly lower than that in the control group ($P < 0.05$). Our research also showed that the activities of caspase-9 and caspase-3 were highly increased in DCM hearts compared with the control values (4.35 ± 0.58 versus 1.12 ± 0.11 and 3.13 ± 0.51 versus 0.98 ± 0.10, respectively, both $P < 0.05$, Fig. 3E). And the myocardial apoptosis degree in the untreated group was similar to that in the control group.

3.7. Alterations of mitochondrial content of STAT3

The mitochondrial content of phosphorylated and total STAT3 in the model group were both significantly decreased compared with the control group ($P < 0.05$). The ratio of phosphorylated STAT3 to total STAT3 in the mitochondrial fraction of DCM hearts was significantly lower than that in the control group ($P < 0.05$, Fig. 4). The mitochondrial content of phosphorylated and total STAT3 and the ratio of phosphorylated STAT3 to total STAT3 did not differ between the untreated and control groups ($P > 0.05$).

4. Discussion

The present study demonstrates that CRT is localized at cardiomyocyte mitochondria and that the mitochondrial content of CRT is enhanced in DCM hearts.

CRT is a Ca^{2+}-binding chaperone of the endoplasmic reticulum [3]. However, it is not only localized in the sarcoplasmic reticulum [3], has also been found in the cytosol [8,9], nucleus [10,11], secretory granules [12,13], cell surface [14], and the extracellular matrix [15]. Nevertheless CRT was not detected in mitochondria isolated from human myocardium using a proteomic approach [20]. In the present study, we identified CRT in mitochondria of rat myocardium using independent techniques such as immune-electron microscopy and Western blot analysis. The immune-electron microscopy demonstrated the presence of colloidal-gold-labeled CRT antibodies within mitochondria. The distribution of the gold-labeled particles was not very high specificity, as the low specificity but high sensitivity of the immune-electron microscopy technique or the CRT antibody. Due to the distance of about 20 nm between the antigen and the gold-labeled particle as well as the high density of membranes in the mitochondria, the exact localization of CRT in mitochondria could not be determined by immune-electron microscopy. Thereby the presence of CRT within mitochondria was confirmed by the Western blot analysis. The CRT protein contains no leader sequence targeting the precursor protein to the mitochondria as analyzed with MITOPORT and TargetP [21,22]. However, it is possible that CRT is imported into the mitochondria via the presequence receptors of the TOM and TIM (translocases of the outer and inner membrane, respectively) protein complexes, which are not necessarily dependent on cleavable presequences [23].

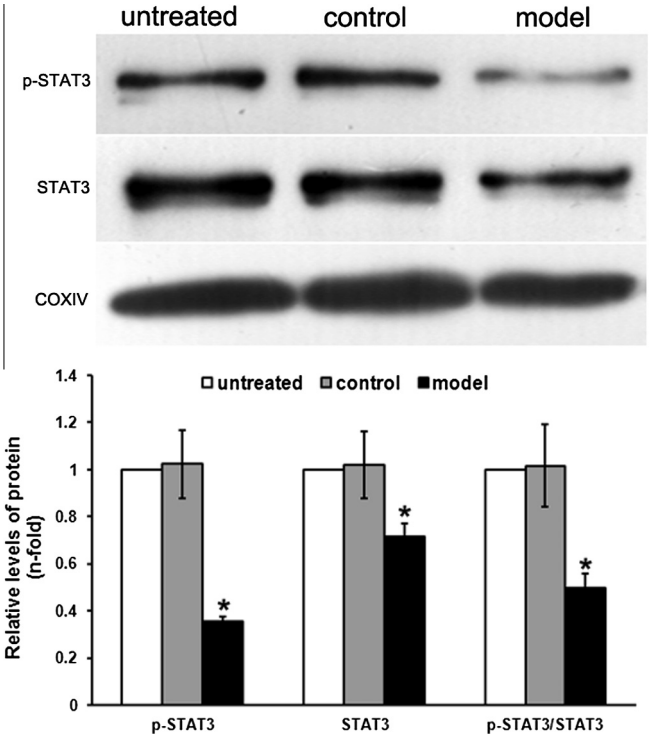

Fig. 4. Alterations of mitochondrial content of STAT3. The protein expression levels of phosphorylated and total STAT3 in cardiac mitochondria were determined by Western blot. COXIV was used as a loading control for the mitochondrial protein. A representative blot is shown in the top panel, and quantitative analysis results are shown in the bottom panel. Data are mean ± SD ($n = 6$, 6 and 10 respectively), and each Western blot was performed in triplicate. *$P < 0.05$ versus the control group.

CRT is highly expressed in the embryonic heart, but immediately down-regulated after birth [4]. The overexpression of CRT in the postnatal heart results in DCM [5]. However, the accurate pathogenesis of CRT in the progress of DCM is still unclear. Previous studies have reported that CRT affects STAT3 signaling and functions as a STAT3 inhibitor [24], and up-regulated expression of CRT in the DCM hearts could inhibit STAT3 phosphorylation [16]. It has also been demonstrated that STAT3 is present in mitochondria [25,26], and mitochondrial STAT3 possibly contributes to cardioprotection by modulation of mitochondrial electron transport chain and inhibition of permeability transition pore opening [27,28]. Our present research revealed that phosphorylated STAT3, total STAT3, and the ratio of phosphorylated to total STAT3 in the mitochondria of DCM hearts were all significantly decreased, suggesting that mitochondrial CRT may directly inhibit mitochondrial STAT3 in the progress of DCM.

Down-regulated expression of STAT3 could reduce its protective effect on cardiac mitochondria. Morphological and functional analysis showed mitochondrial injury in the DCM hearts. Our data also illustrated the more release of cytochrome c from mitochondria, activation of caspase-9 and caspase-3, and the increased apoptosis index, suggesting the mitochondrial related apoptosis pathway occurred in the DCM hearts. And further studies have showed that the mitochondrial content of CRT had negative correlations with

mitochondrial function, and a positive correlation with myocardial apoptosis index, suggesting that up-regulated mitochondrial CRT could lead to serious cardiac mitochondrial damage and the myocardial apoptosis.

In summary, CRT is also present in cardiomyocyte mitochondria, and its protein expression level is increased in DCM hearts. Up-regulated expression of mitochondrial CRT may lead to serious cardiac mitochondrial damage through inhibiting the phosphorylation of mitochondrial STAT3. However, the exact mitochondrial location of CRT and its importing mechanism to mitochondria will be further explored in our future studies.

Conflict of interest

The authors declare that there are no conflicts of interest with this work.

Acknowledgments

This study were supported by grants from National Natural Science Foundation of China (No. 81170209 to J.W.), and Specialized Research Fund for the Doctoral Program of Higher Education of China (No. 20100201120065 to J.H.X.).

References

[1] J.L. Jefferies, J.A. Towbin, Dilated cardiomyopathy, Lancet 375 (2010) 752–762.
[2] E. Arbustini, M. Diegoli, R. Fasani, M. Grasso, P. Morbini, et al., Mitochondrial DNA mutations and mitochondrial abnormalities in dilated cardiomyopathy, Am. J. Pathol. 153 (1998) 1501–1510.
[3] M. Michalak, J. Groenendyk, E. Szabo, L.I. Gold, M. Opas, Calreticulin, a multi-process calcium-buffering chaperone of the endoplasmic reticulum, Biochem. J. 417 (2009) 651–666.
[4] N. Mesaeli, K. Nakamura, E. Zvaritch, P. Dickie, E. Dziak, et al., Calreticulin is essential for cardiac development, J. Cell. Biol. 144 (1999) 857–868.
[5] D. Lee, T. Oka, B. Hunter, A. Robinson, S. Papp, et al., Calreticulin induces dilated cardiomyopathy, PLoS One 8 (2013) e56387.
[6] M. Meyer, W. Schillinger, B. Pieske, C. Holubarsch, C. Heilmann, et al., Alterations of sarcoplasmic reticulum proteins in failing human dilated cardiomyopathy, Circulation 92 (1995) 778–784.
[7] O. Suzuki, T. Kanai, T. Nishikawa, Y. Yamamoto, A. Noguchi, et al., Adult onset cardiac dilatation in a transgenic mouse line with Galbeta1,3GalNAc alpha2,3-sialyltransferase II (ST3Gal-II) transgenes: a new model for dilated cardiomyopathy, Proc. Jpn. Acad. Ser. B Phys. Biol. Sci. 87 (2011) 550–562.
[8] N. Afshar, B.E. Black, B.M. Paschal, Retrotranslocation of the chaperone calreticulin from the endoplasmic reticulum lumen to the cytosol, Mol. Cell. Biol. 25 (2005) 8844–8853.
[9] C.A. Labriola, I.L. Conte, M. Lopez Medus, A.J. Parodi, J.J. Caramelo, Endoplasmic reticulum calcium regulates the retrotranslocation of *Trypanosoma cruzi* calreticulin to the cytosol, PLoS One 5 (2010) e13141.
[10] Y.H. Huh, S.H. Yoo, Presence of the inositol 1,4,5-triphosphate receptor isoforms in the nucleoplasm, FEBS Lett. 555 (2003) 411–418.
[11] J.M. Holaska, B.E. Black, D.C. Love, J.A. Hanover, J. Leszyk, et al., Calreticulin is a receptor for nuclear export, J. Cell Biol. 152 (2001) 127–140.
[12] C. Andrin, M.J. Pinkoski, K. Burns, E.A. Atkinson, O. Krahenbuhl, et al., Interaction between a Ca^{2+}-binding protein calreticulin and perforin, a component of the cytotoxic T-cell granules, Biochemistry 37 (1998) 10386–10394.
[13] S.A. Fraser, R. Karimi, M. Michalak, D. Hudig, Perforin lytic activity is controlled by calreticulin, J. Immunol. 164 (2000) 4150–4155.
[14] A. Vaithilingam, J.E. Teixeira, P.J. Miller, B.T. Heron, C.D. Huston, *Entamoeba histolytica* cell surface calreticulin binds human C1q and functions in amebic phagocytosis of host cells, Infect. Immun. 80 (2012) 2008–2018.
[15] E. Somogyi, U. Petersson, K. Hultenby, M. Wendel, Calreticulin – an endoplasmic reticulum protein with calcium-binding activity is also found in the extracellular matrix, Matrix Biol. 22 (2003) 179–191.
[16] M. Zhang, J. Wei, H. Shan, H. Wang, Y.H. Zhu, et al., Calreticulin-STAT3 signaling pathway modulates mitochondrial function in a rat model of furazolidone-induced dilated cardiomyopathy, PLoS One 8 (2013) e66779.
[17] K.S. Dujardin, C. Tei, T.C. Yeo, D.O. Hodge, A. Rossi, et al., Prognostic value of a Doppler index combining systolic and diastolic performance in idiopathic-dilated cardiomyopathy, Am. J. Cardiol. 82 (1998) 1071–1076.
[18] K. Boengler, G. Dodoni, A. Rodriguez-Sinovas, A. Cabestrero, M. Ruiz-Meana, et al., Connexin 43 in cardiomyocyte mitochondria and its increase by ischemic preconditioning, Cardiovasc. Res. 67 (2005) 234–244.
[19] E.L. Holmuhamedov, S. Jovanovic, P.P. Dzeja, A. Jovanovic, A. Terzic, Mitochondrial ATP-sensitive K+ channels modulate cardiac mitochondrial function, Am. J. Physiol. 275 (1998) H1567–H1576.
[20] S.W. Taylor, E. Fahy, B. Zhang, G.M. Glenn, D.E. Warnock, et al., Characterization of the human heart mitochondrial proteome, Nat. Biotechnol. 21 (2003) 281–286.
[21] M.G. Claros, P. Vincens, Computational method to predict mitochondrially imported proteins and their targeting sequences, Eur. J. Biochem. 241 (1996) 779–786.
[22] O. Emanuelsson, H. Nielsen, S. Brunak, G. von Heijne, Predicting subcellular localization of proteins based on their N-terminal amino acid sequence, J. Mol. Biol. 300 (2000) 1005–1016.
[23] T. Endo, H. Yamamoto, M. Esaki, Functional cooperation and separation of translocators in protein import into mitochondria, the double-membrane bounded organelles, J. Cell Sci. 116 (2003) 3259–3267.
[24] H. Coe, J. Jung, J. Groenendyk, D. Prins, M. Michalak, ERp57 modulates STAT3 signaling from the lumen of the endoplasmic reticulum, J. Biol. Chem. 285 (2010) 6725–6738.
[25] J. Wegrzyn, R. Potla, Y.J. Chwae, N.B. Sepuri, Q. Zhang, et al., Function of mitochondrial Stat3 in cellular respiration, Science 323 (2009) 793–797.
[26] P. Tammineni, C. Anugula, F. Mohammed, M. Anjaneyulu, A.C. Larner, et al., The import of the transcription factor STAT3 into mitochondria depends on GRIM-19, a component of the electron transport chain, J. Biol. Chem. 288 (2013) 4723–4732.
[27] K. Szczepanek, Q. Chen, A.C. Larner, E.J. Lesnefsky, Cytoprotection by the modulation of mitochondrial electron transport chain: the emerging role of mitochondrial STAT3, Mitochondrion 12 (2012) 180–189.
[28] K. Boengler, D. Hilfiker-Kleiner, G. Heusch, R. Schulz, Inhibition of permeability transition pore opening by mitochondrial STAT3 and its role in myocardial ischemia/reperfusion, Basic Res. Cardiol. 105 (2010) 771–785.